the plant journal

SEB SOCIETY FOR EXPERIMENTAL BIOLOGY

The Plant Journal (2008) **55**, 478–490 doi: 10.1111/j.1365-313X.2008.03522.x

Inter-dependence of dimerization and organelle binding in myosin XI

Jian-Feng Li* **and Andreas Nebenführ**

Department of Biochemistry, Cellular and Molecular Biology, University of Tennessee, Knoxville, TN 37996-0840, USA

Received 10 March 2008; accepted 3 April 2008; published online 2 June 2008.
*For correspondence (fax +1 865 974 6306; e-mail jli28@utk.edu).

Summary

Cytoplasmic streaming is a ubiquitous process in plant cells that is thought to be driven by the active movement of myosin XI motor proteins along actin filaments. These myosin motors bind to organelles through their C-terminal globular tail domain, although recent studies have also suggested a role for the central coiled-coil region during organelle binding. Here we have investigated the relationship between these two protein domains of MYA1, an Arabidopsis myosin XI, in a series of *in vivo* experiments demonstrating that dimerization of the coiled-coil region stabilizes organelle binding of the globular tail. Surprisingly, yeast two-hybrid assays, bimolecular fluorescence complementation, Förster resonance energy transfer and *in vitro* pull-down experiments all demonstrated that dimerization of the 174-residue MYA1 coiled coils by themselves was unstable. Furthermore, only the first of the two major coiled-coil segments in MYA1 contributed significantly to dimer formation. Interestingly, dimerization of myosin tail constructs that included the organelle-binding globular tail was stable, although the globular tails by themselves did not interact. This suggests an inter-dependent relationship between dimerization and organelle binding in myosin XI, whereby each process synergistically stimulates the other.

Keywords: myosin XI, coiled-coil region, dimerization, organelle targeting, bimolecular fluorescence complementation, Förster resonance energy transfer.

Introduction

Cytoplasmic streaming is a prominent process in plant cells that is characterized by the rapid movement of organelles throughout the cell (Shimmen, 2007). These movements occur along cytoskeletal actin filaments and are driven by plant myosins (Jedd and Chua, 2002; Nebenführ *et al.*, 1999; Van Gestel *et al.*, 2002) bound to the surface of organelles (Hashimoto *et al.*, 2005; Li and Nebenführ, 2007; Reisen and Hanson, 2007; Romagnoli *et al.*, 2007; Wang and Pesacreta, 2004). Given the high energy expenditure required to keep cytoplasmic streaming active, it is reasonable to assume that this activity performs important physiological functions. For example, organelle movements may lead to the constant mixing of cytoplasm (Houtman *et al.*, 2007), which in turn results in an even distribution of small metabolites in the cell that may be necessary for cell growth (Shimmen and Yokota, 1994). Indeed, loss of a single myosin gene results in reduced growth of root hairs even though cytoplasmic streaming is not completely eliminated in these mutants (Ojangu *et al.*, 2007; Peremyslov *et al.*, 2008). At the same time, it is thought that cytoplasmic streaming is responsible for the delivery of organelles to specific positions in polarized cells. For example, secretory vesicles accumulate in the tip region of pollen tubes and root hairs after moving through the length of the cell (Cole and Fowler, 2006). Direct evidence for either of these functions is still lacking, and a better understanding of the motor mechanisms as well as their regulation during organelle movements is required.

Myosins are nanoscale motor proteins that move along actin filaments in eukaryotic cells by utilizing the energy from ATP hydrolysis (Krendel and Mooseker, 2005). Based on sequence similarity of the highly conserved motor domain, myosin genes have been categorized into 24 sub-families designated class I–XXIV (Foth *et al.*, 2006). Plants exclusively possess class VIII and XI myosins (Reddy and Day, 2001), with the majority of genes falling into the latter sub-family. In particular, Arabidopsis encodes 13 myosin XI isoforms but only four myosin VIII isoforms, while rice expresses 12 myosin class XI isoforms and only two in

class VIII (Jiang and Ramachandran, 2004; Reddy and Day, 2001). This discrepancy in paralog number may indicate the significance of the myosin XI sub-family in plant physiology. While class VIII myosins appear to be involved in the maturation of new cell plates and in intercellular communication (Reichelt *et al.*, 1999), class XI myosins are believed to drive organelle movements during plant cytoplasmic streaming (Li and Nebenführ, 2008).

Similar to myosin V in animals and fungi, plant myosin XI has a domain structure that is well-adapted to power organelle trafficking in the cell. All myosin XI isoforms contain a catalytic motor domain at the N-terminus that binds to actin filament and hydrolyzes ATP (Kinkema and Schiefelbein, 1994; Tominaga *et al.*, 2003). After the motor domain are six contiguous IQ motifs, which act as a lever arm and whose association with calmodulin-like proteins regulates the mechanical performance of the motor (Kinkema and Schiefelbein, 1994). The C-terminal region of myosin XI is known as the globular tail, which binds to cellular cargoes (Li and Nebenführ, 2007). Between the sixth IQ motif and the globular tail lies a coiled-coil region that is generally believed to dimerize two myosin molecules (Kinkema and Schiefelbein, 1994). This predicted dimerization would permit the hand-over-hand movement of the two connected motor domains with a 35 nm step size, as observed in laser-trap experiments (Tominaga *et al.*, 2003). These large steps match the half-pitch of an actin helix, and thus avoid spiraling of the entire traffic complex around actin filaments. At the same time, dimerization of two myosin XI heavy chains would probably enable organelle binding by two globular tails, thus allowing the processive movement of an organelle tightly attached to the globular tails.

Although the dimerization of myosin XI by its coiled-coil region has been taken for granted since the cloning of the first myosin XI gene, it is just an *in silico* prediction based on the primary sequence. The only available experimental evidence for myosin XI dimerization via the coiled-coil region is the determination of the morphology of purified myosin XI by rotary-shadowed electron microscopy (Tominaga *et al.*, 2003). Direct *in vivo* evidence for dimerization has been lacking, and the detailed features of the myosin XI coiled-coil region as well as its role in myosin function have not been characterized.

In a previous study, we identified two interacting sub-domains within the globular tail of myosin XI. Each globular tail sub-domain on its own is targeting-competent, suggesting that the globular tail is the cargo-binding domain and possesses at least two separate binding sites (Li and Nebenführ, 2007). Surprisingly, overexpressed full-length globular tails of several myosin XI isoforms failed to target to organelles (Li and Nebenführ, 2007; Reisen and Hanson, 2007), which may have been due to compromised regulation of an allosteric interaction between the two globular tail sub-domains (Li and Nebenführ, 2007). By contrast, constructs including both the coiled-coil region and the globular tail could target to organelles reliably (Li and Nebenführ, 2007; Reisen and Hanson, 2007), indicative of an involvement of the coiled-coil region in the organelle binding of myosin XI. In this study, we examined the relationship between the coiled-coil region and the globular tail of MYA1, a myosin XI isoform of Arabidopsis. As detection of targeting competence requires measurements in intact plant cells, we performed transient expression analysis of a large number of fluorescently labeled constructs followed by live-cell imaging. Transient assays are expected to yield reliable localization information (Goodin *et al.*, 2007) and avoid potential deleterious dominant-negative effects (Avisar *et al.*, 2008). We first sought to determine how the coiled-coil region of MYA1 affects targeting by the globular tail. Furthermore, we tested whether the coiled-coil region of MYA1 mediates dimerization, and, more importantly, how this dimerization is stabilized. Taken together, our experimental data demonstrate that dimerization and organelle targeting are synergistically coordinated in myosin XI.

Results

The coiled-coil region of MYA1 consists of two major coiled-coil segments

The coiled coil is a common protein structural motif that is usually associated with protein oligomerization and is present in about 6% of all proteins encoded by the Arabidopsis genome (Rose *et al.*, 2004). The characteristic feature of coiled coils is a seven-residue (heptad) sequence unit denoted as '*abcdefg*', where the *a* and *d* positions are occupied by hydrophobic residues and the *e* and *g* positions are occupied by charged or polar residues (Mason and Arndt, 2004). In order to precisely identify the residues likely to be involved in coiled-coil formation in MYA1, we employed two prediction algorithms, COILS (Lupas *et al.*, 1991) and Paircoil2 (McDonnell *et al.*, 2006). Both algorithms identified two major segments of coiled-coil structures in MYA1 (Figure S1a), which was also true for other plant myosin XI isoforms (data not shown). Based on these predictions and additional considerations (see Appendix S1), the two coiled-coil sections of MYA1 were identified as residues Leu874 to Ala951 and residues Asp967 to Gln1047 (Figure 1a), respectively, interrupted by a predicted 15-residue non-helical loop (Figure 1a). Given that each residue in an α-helix extends for 0.15 nm, the whole predicted coiled-coil region of MYA1 has a deduced length of 23.9 nm, which closely matches the stalk length of 25 nm in a tobacco myosin XI isoform visualized by electron microscopy (Tominaga *et al.*, 2003).

Multiple sequence alignment revealed that the coiled-coil region of myosin XI was highly conserved among various monocotyledonous and dicotyledonous species, except for

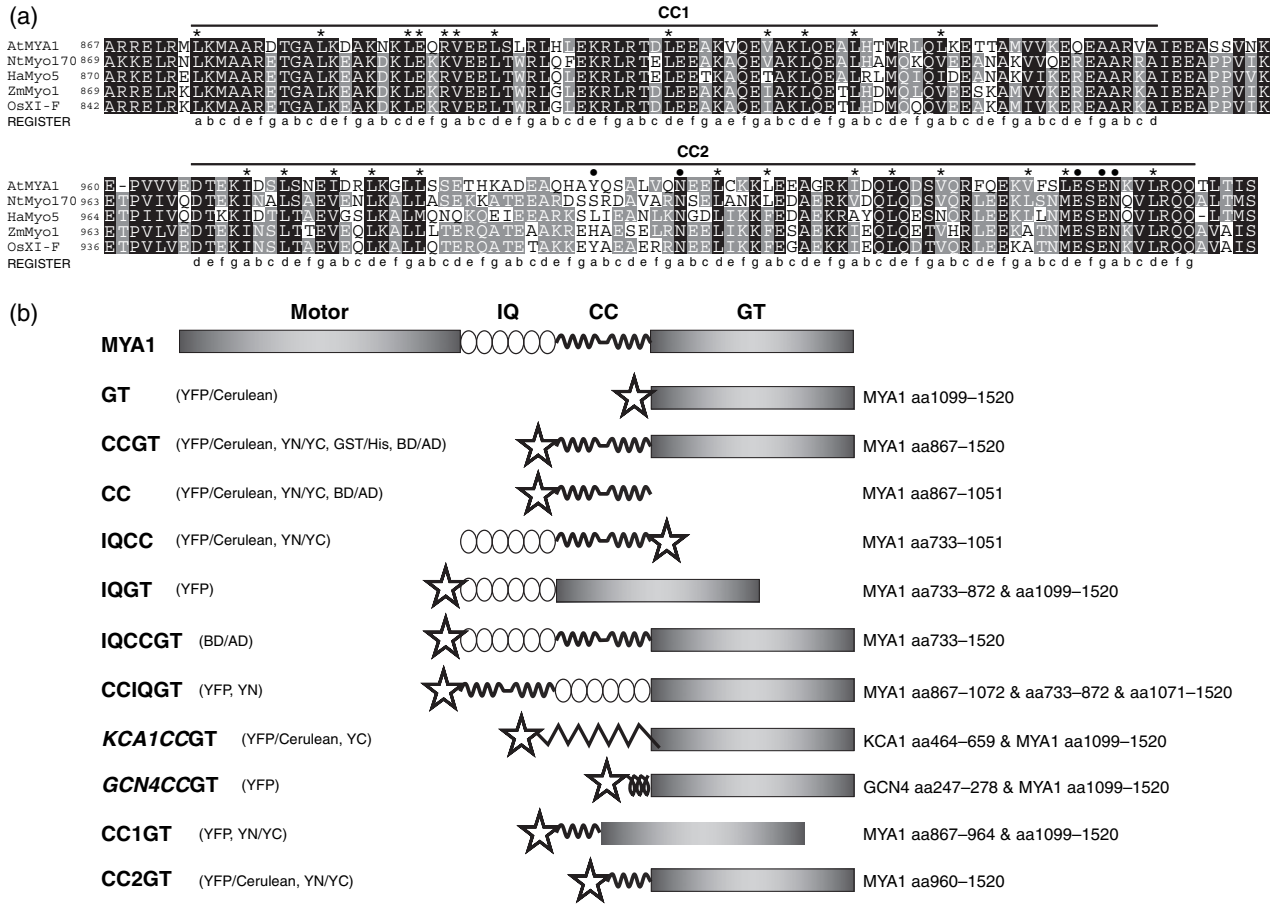

Figure 1. The coiled-coil region of myosin XI contains two major coiled-coil sections.
(a) Multiple sequence alignment of the coiled-coil region of myosin XI from various plant species, namely *Arabidopsis thaliana* AtMYA1 (NM_101620), *Nicotiana tabacum* NtMyo170 (BAD72949), *Helianthus annuus* HaMyo5 (AAB71529), *Zea mays* ZmMyo1 (AAD17931) and *Oryza sativa* OsXI-F (NP_001057670). The two major coiled-coil sections are individually labeled as CC1 and CC2. The position of each amino acid within the heptad register of AtMYA1 coiled-coil region is indicated by a letter from *a* to *g*. Residues predicted to stabilize or to destabilize the coiled-coil dimerization are marked by asterisks or dots, respectively.
(b) Schematic diagram of MYA1 constructs used in this study. The star in each construct represents the fusion tag(s) indicated after the name of the construct. The length of individual domains in each construct is indicated on the right. A diagram for YFP–GTplus (MYA1 amino acids 1052–1520) construct is not included as it has an identical domain structure to YFP–GT.

a short stretch of residues in the middle of the second coiled-coil section (Figure 1a). In particular, the probable orthologs of MYA1 from *Nicotiana tabacum*, *Helianthus annuus*, *Zea mays* and *Oryza sativa* exhibited identity/similarity of 63/83%, 57/81%, 64/83% or 65/83%, respectively, to MYA1 within the equivalent region. More importantly, 87% of the residues at the core (*a* and *d*) positions and 76% of the residues at the *e* and *g* positions were conserved (Figure 1a), suggesting that the coiled-coil regions of all plant myosin XIs may function similarly.

The presence of the coiled-coil region facilitates MYA1 targeting

Recent studies have demonstrated that the presence of the coiled-coil region is essential for stable targeting of myosin XI to organelles (Li and Nebenführ, 2007; Reisen and Hanson, 2007), although the globular tail of myosin XI by itself carries sufficient targeting information (Li and Nebenführ, 2007). To elucidate the underlying mechanisms, we transiently expressed a series of YFP-tagged MYA1 deletions (Figure 1b) in Arabidopsis leaf epidermis to compare their targeting behaviors. We carefully evaluated at least 60 cells from three independent transformations for each construct, and consistently found the same localization pattern for a given construct. In agreement with our previous study (Li and Nebenführ, 2007), the globular tail by itself (YFP–GT) or a version that was 47 residues longer and truncated after the coiled-coil region (YFP–GTplus) both showed cytoplasmic distribution (Figure 2a,b). By contrast, a construct containing the coiled-coil region and the globular tail (YFP–CCGT) routinely labeled punctate structures undergoing oscillatory or stop-and-go movements in the cytosol, indicative of organelle binding (Figure 2c). In addition, we also

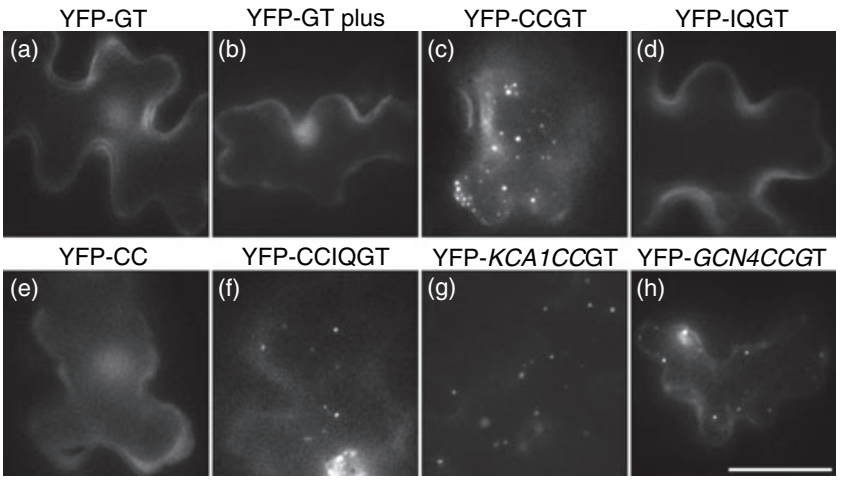

Figure 2. Stable targeting of the MYA1 globular tail requires the presence of the coiled-coil region.
All constructs were observed in Arabidopsis leaf epidermal cells following transient expression after particle bombardment. Scale bar = 20 μm.
(a, b, d, e) YFP–GT, YFP–GTplus, YFP–IQGT and YFP–CC showed diffuse cytoplasmic distribution.
(c, f, g, h) YFP–CCGT, YFP–CCIQGT, YFP–KCA1 CCGT and YFP–GCN4CCGT labeled punctate structures in the cytosol.

tested the equivalent GT and CCGT constructs of three other myosin XI isoforms in Arabidopsis, namely MYA2, XI-I and XI-K, and observed the same targeting behaviors as the MYA1 constructs in all cases (Figure S2).

In principle, stimulation of organelle binding by the coiled-coil domain could be mediated by several mechanisms. For example, recovery of globular tail targeting in YFP–CCGT constructs could be a general consequence of the addition of α-helical sequences N-terminal to the globular tail. However, a construct with the six α-helical IQ motifs fused to the N-terminus of the globular tail (YFP–IQGT) showed only diffuse cytoplasmic labeling (Figure 2d), suggesting that the coiled-coil region plays a specific role in organelle targeting. This specific function could involve direct binding of the coiled-coil region to the organelle. However, when a construct consisting only of the coiled-coil region (YFP–CC) was expressed, again only diffuse fluorescence in the cytoplasm could be observed (Figure 2e). In order to investigate whether organelle targeting involves a direct interaction between the coiled coils and the globular tail, a chimeric construct, YFP–CCIQGT, was tested, in which the coiled-coil region and the globular tail were separated by a 20 nm rigid spacer (i.e. six IQ motifs). This chimeric construct could still label specific puncta in the cytoplasm (Figure 2f), suggesting that direct communication between the coiled-coil region and the globular tail is not necessary for targeting, as this extended IQ spacer should have been long enough to block any potential interaction between these two domains.

Finally, it is conceivable that the coiled-coil region may indirectly affect organelle binding of the globular tail by dimerization. To test whether this is the case, the MYA1 coiled-coil region in the CCGT construct was substituted with an unrelated coiled-coil region from Arabidopsis kinesin KCA1, which has been shown to mediate dimerization of this microtubule-based motor (Vanstraelen *et al.*, 2004). Indeed, the YFP–KCA1CCGT chimeric construct performed the targeting as well as the MYA1 CCGT construct (Figure 2g). Furthermore, when the strongly dimerizing 32-residue coiled coil from the yeast transcriptional activator GCN4 (Kammerer *et al.*, 1998) was introduced instead of the 174-residue MYA1 coiled-coil region in the CCGT construct, the resulting YFP–GCN4CCGT construct also readily bound to organelles (Figure 2h). Thus, our data strongly suggested that the coiled-coil region of MYA1 affects globular tail targeting by homodimerization.

The coiled-coil region of MYA1 mediates its dimerization in living plant cells

To date, experimental evidence for the dimerization of myosin XI coiled-coil regions is limited to determination of the morphology of purified tobacco myosin XI under the electron microscope, which suggests an association of two myosin heavy chains through their central domains (Tominaga *et al.*, 2003). We sought to provide direct experimental confirmation of coiled coil-mediated MYA1 dimerization by examining protein–protein interactions.

Dimerization of the MYA1 coiled-coil region was first tested in a yeast two-hybrid system (Y2H), which has been successfully utilized in the past to detect coiled-coil interactions (e.g. Vanstraelen *et al.*, 2004). Homodimerization between three types of MYA1 truncations was tested, containing the entire coiled-coil region but different neighboring domains. The shortest construct contained only the coiled-coil region (CC), a second one included the coiled-coil region plus the globular tail (CCGT), while the longest one spanned from the IQ motifs to the globular tail (IQCCGT). Unexpectedly, none of these constructs exhibited positive interactions with themselves in the Y2H system (Figure 3a).

These results might be explained by a lack of plant-specific co-factor(s) that may be necessary for stable MYA1 dimerization as described for a myosin V isoform (Wagner

(a)

Constructs	β-gal
CC	–
CCGT	–
IQCCGT	–

(b)

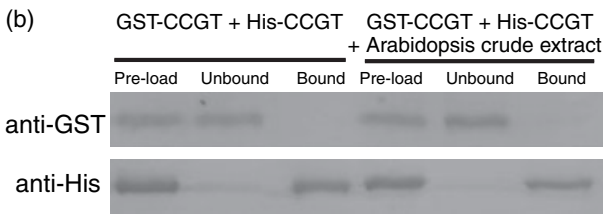

Figure 3. The coiled-coil region of MYA1 is incapable of dimerization in a yeast two-hybrid system and *in vitro*.
(a) Yeast two-hybrid assay for homodimerization between CC, CCGT and IQCCGT constructs. The lack of a color reaction in the β-galactosidase assay is indicated by '–'.
(b) *In vitro* pull-down assay of *E. coli*-expressed tail constructs. 'Pre-load' lanes show input protein levels of His-tagged CCGT and GST-tagged CCGT. 'Unbound' lanes identify proteins remaining in supernatant above Ni-NTA resin. 'Bound' lanes contain proteins that could be precipitated with Ni-NTA resin. The left and right three lanes show experiments performed in the absence or presence of Arabidopsis crude protein extracts, respectively.

et al., 2006). To investigate this possibility, we expressed GST-tagged and His-tagged CCGT proteins separately in *Escherichia coli*, and tested for their interaction by an *in vitro* pull-down assay. As expected from the Y2H results, the GST-tagged CCGT protein could not be co-purified with the His-tagged CCGT protein using His-tag binding resin (Figure 3b). Addition of Arabidopsis crude protein extracts did not result in a detectable interaction between GST-tagged CCGT and His-tagged CCGT proteins (Figure 3b). These results suggest that the coiled-coil region of MYA1 is incapable of forming homodimers in yeast or *in vitro*.

We next performed bimolecular fluorescence complementation (BiFC) assays to study whether dimerization of the MYA1 coiled-coil region is possible in Arabidopsis leaf epidermal cells. BiFC relies on formation of an active fluorophore (YFP) from its two halves [N-terminal YFP (YN) and C-terminal YFP (YC)] when they are brought into direct contact by stable interaction between their fusion partners (Hu *et al.*, 2002). As a positive control, the BiFC combination of YN–GCN4CC and YC–GCN4CC, both containing the autonomously dimerizing GCN4 leucine zipper (Kammerer *et al.*, 1998), demonstrated restored YFP fluorescence in the cytoplasm and nucleus (Figure 4a), resembling the distribution of intact YFP in the cell. By contrast, the MYA1 combinations of YN–CC and YC–CC or IQCC–YN and IQCC–YC did not show any restored YFP fluorescence within 100 cells expressing the transformation indicator, a CFP-tagged peroxisome marker (Figure 4b,c), suggesting that dimerization between MYA1 coiled-coil regions by themselves does not occur or is unstable. However, the combination of YN–CCGT and YC–CCGT clearly generated reconstituted YFP signal targeted to organelles (Figure 4d), in this case peroxisomes due to co-localization of YFP signal with CFP-labeled peroxisomes (data not shown). This result suggests that stable dimerization could occur between CCGT constructs. When the MYA1 coiled-coil region of the YC–CCGT construct in the above combination was replaced by the KCA1 coiled-coil region, no reconstituted YFP signal was detected in 100 cells expressing the transformation marker (Figure 4e), although both constructs are known to target to organelles (Figure 2c,g). Identical observations were obtained after transient expression of these constructs in tobacco leaf epidermis (Figure S3). Together, these results suggested that the CCGT construct contains all regions necessary for efficient MYA1 dimerization in living plant cells, and that this dimerization is mediated by the coiled-coil region rather than the globular tail.

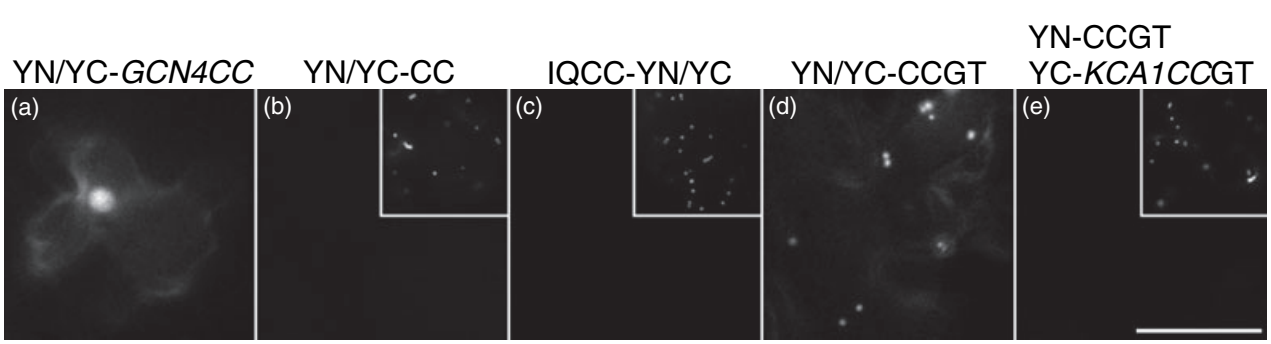

Figure 4. The coiled-coil region of MYA1 can dimerize in the BiFC assay in Arabidopsis leaf epidermis.
(a) Restored YFP fluorescence was detected in the BiFC combination YN–GCN4CC + YC–GCN4CC.
(b, c, e) No restored YFP fluorescence was detected in MYA1 BiFC combinations YN–CC + YC–CC, IQCC–YN + IQCC–YC and YN–CCGT + YC–KCA1CCGT, respectively. The insets show peroxisome-labeling CFP fluorescence in the same cells as the transformation marker at half scale.
(d) Restored YFP fluorescence was detected in the MYA1 BiFC combination YN–CCGT + YC–CCGT.
All construct combinations were observed following transient expression after particle co-bombardment. Scale bar = 20 μm.

As the BiFC assay is unable to detect weak interactions, we carried out Förster resonance energy transfer (FRET) assays in living plant cells to further characterize the dimerization of the MYA1 coiled-coil region. FRET is based on changes in the fluorescence intensities or lifetimes of two fluorophores (i.e. YFP and Cerulean, a brighter CFP variant; Rizzo *et al.*, 2004) when they are brought into close proximity by interaction between their fusion partners (Dixit *et al.*, 2006). Thus, FRET has a much higher sensitivity to protein–protein interactions than BiFC. To quantify the dimerization intensity of each FRET combination in at least 45 transformed cells from three separate experiments, we employed a three-image FRET approach in combination with the N_{FRET} (normalized FRET) algorithm, which corrects for variable protein expression levels and cross-talk between fluorescence channels (Xia and Liu, 2001). To establish the validity of this approach in our system, a pair of controls (YFP + Cerulean as the negative control and a YFP–Cerulean fusion with a 10-residue linker as the positive control) were tested, which respectively exhibited no or strong Nfret signal (Figure 5a,b). However, the Nfret signal of the positive control (YFP–Cerulean) reflected the intensity of a direct physical connection and thus could not be used to judge whether an interaction with a lower Nfret signal represented a reversible protein–protein interaction. To this end, the previously reported KCA1 coiled-coil region (Vanstraelen

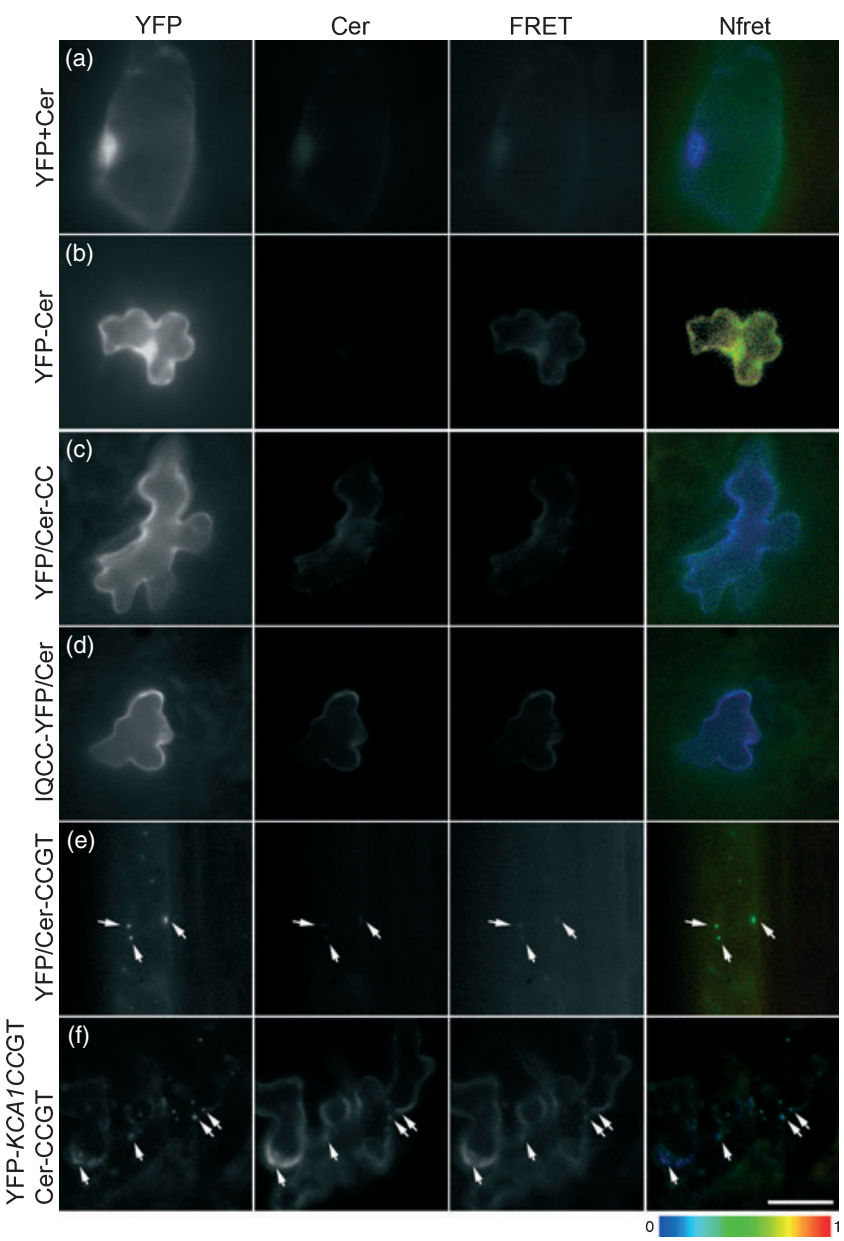

Figure 5. Dimerization of MYA1 coiled-coil constructs can be detected by the FRET assay in Arabidopsis leaf epidermis.
Three images with filter combinations for YFP excitation and YFP emission (YFP), Cerulean excitation and Cerulean emission (Cer), and Cerulean excitation and YFP emission (FRET) were taken, and pixel intensities were used to calculate a normalized FRET value (Nfret), which is color-coded from blue (Nfret = 0) to red (Nfret = 1).
(a) Expression of soluble YFP and Cerulean proteins gave diffuse labeling throughout cytosol and nucleus but did not result in an Nfret signal (blue color).
(b) A covalent YFP–Cerulean fusion led to high Nfret values (green–yellow color).
(c) Combination of YFP–CC and Cerulean-CC resulted in diffuse labeling with low Nfret values (blue color).
(d) IQCC–YFP and IQCC–Cerulean also gave diffuse labeling and low Nfret values (blue color).
(e) Expression of YFP–CCGT and Cerulean–CCGT yielded distinctly labeled structures (arrows) with a relatively high Nfret value (green color).
(f) Combination of YFP–KCA1CCGT and Cerulean–CCGT produced punctate structures (arrows) with low Nfret values (blue color).
In (b) and (e), the Cerulean signal is very weak due to energy transfer from Cerulean to YFP. Scale bar = 20 μm.

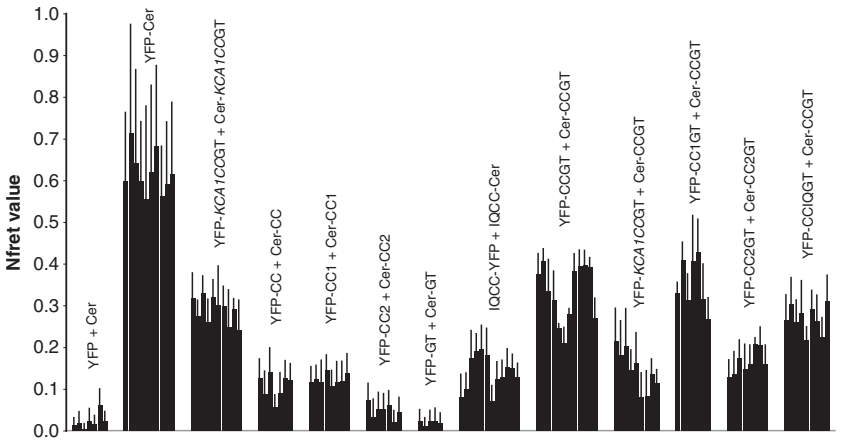

Figure 6. Quantification of Nfret values reveals different levels of interaction strength.
Each bar indicates the average Nfret value from a representative area in a single cell that has substantial image signals in all three channels (YFP, Cerulean and FRET; see Figure 5). Error bars indicate the standard deviation of Nfret values in the selected area. Each group of bars represents the Nfret value of a number of independent cells expressing the indicated combination of YFP and Cerulean constructs. Note that the cell-to-cell variation for a given construct combination is generally less than the variation between construct combinations.

et al., 2004) was used as a specific positive control in a combination of YFP–KCA1CCGT and Cerulean–KCA1CCGT, both of which include the KCA1 coiled-coil region (KCA1CC) and the MYA1 globular tail (GT). As expected, this specific positive control showed an Nfret value that was lower than that of the general positive control (YFP–Cerulean) but significantly higher than that of the negative control (Figure 6).

When YFP–CC and Cerulean–CC were co-expressed in Arabidopsis leaf epidermis, only a weak Nfret signal was detected, which was much lower than that of the specific positive control but about three times as high as that of the negative control (Figures 5c and 6), indicative of a weak interaction between two CC constructs. By contrast, the constitutive interaction between YFP–GCN4CC and Cerulean–GCN4CC was reflected by a higher Nfret signal, although slightly lower than that of the specific positive control (data not shown). The addition of IQ motifs to the N-terminus of the coiled-coil region (IQCC–YFP and IQCC–Cerulean) enhanced the Nfret signal marginally, but it was still lower than that of the specific positive control (Figures 5d and 6). Interestingly, addition of the globular tail to the C-terminus of the coiled-coil region (YFP–CCGT and Cerulean–CCGT) dramatically increased the Nfret signal to a level similar to that of the specific positive control (Figures 5e and 6), indicative of a stable interaction between two CCGT constructs. When the MYA1 coiled-coil region of the YFP–CCGT construct in the above combination was substituted by the KCA1 coiled-coil region, the Nfret signal was found to be drastically reduced, although both constructs localized to the same organelles (Figures 5f and 6). Similar results were achieved when these FRET assays were repeated in tobacco leaf epidermis (Figure S4). Consistent with the BiFC assays, the results from FRET assays again suggested that the stable interaction between CCGT constructs was specifically dependent on the coiled-coil region rather than the globular tail. In addition, the FRET data highlighted that there was a weak interaction between the coiled-coil regions by themselves, which could not be detected by any of the other assays.

The first coiled-coil segment determines the overall stability of MYA1 coiled-coil dimerization

To determine the contribution of individual coiled-coil segments of MYA1 to the dimerization, we removed the first and second coiled-coil segments, respectively, from the CCGT construct to investigate their effects on MYA1 dimerization. Interestingly, absence of the second coiled-coil segment from the CCGT construct still allowed a stable dimerization between CC1GT and CCGT constructs to occur in both FRET (Figure 6) and BiFC assays (Figure 7a). In addition, a restored YFP signal could also be detected in the BiFC assay for the YN–CC1GT and YC–CC1GT combination (Figure 7b). By contrast, there was no detectable YFP fluorescence for the BiFC combination of YN–CC2GT and YC–CCGT in more than 100 cells expressing the CFP transformation indicator (Figure 7c). Similarly, removal of the first coiled-coil segment from the CCGT construct severely destabilized the self-interaction between two CC2GT constructs in both FRET (Figure 6) and BiFC assays (Figure 7d). More importantly, the interaction between CC1GT and CCGT constructs had a similar Nfret intensity as that between two CCGT constructs (Figure 6). Even in the absence of the globular tail, the self-interaction of CC1 was as strong as that of the entire coiled-coil region, and much stronger than that of CC2 (Figure 6). Taken together, these experimental data strongly imply that the first coiled-coil segment (CC1) determines the overall stability of MYA1 coiled-coil homodimerization.

Globular tail targeting stabilizes MYA1 coiled-coil dimerization

Our BiFC and FRET data raised the interesting question as to why dimerization between CCGT constructs was stable while that between CC or IQCC constructs were not. The

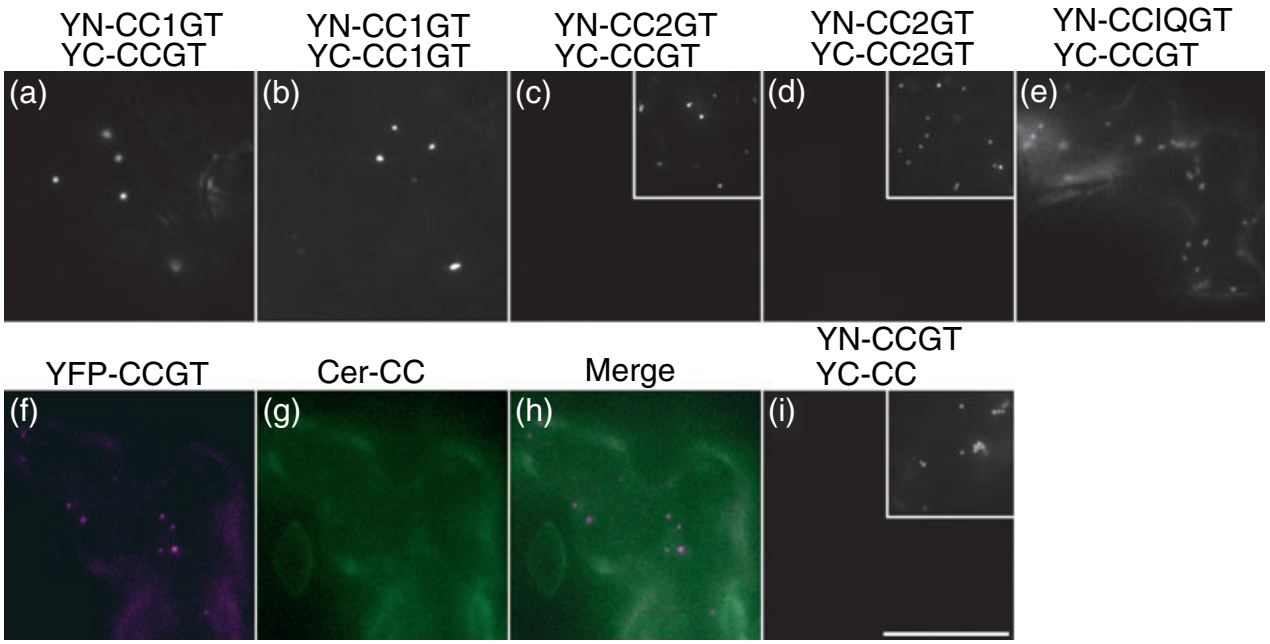

Figure 7. The first coiled-coil section determines the stability of MYA1 dimer, which in turn depends on organelle binding of two globular tails.
(a, b) Restored YFP fluorescence was detected in the BiFC combinations YN–CC1GT + YC–CCGT and YN–CC1GT + YC–CC1GT.
(c, d) No restored YFP fluorescence was detected in the BiFC combinations YN–CC2GT + YC–CCGT and YN–CC2GT + YC–CC2GT.
(e) Restored YFP fluorescence was detected in BiFC combination YN–CCIQGT + YC–CCGT.
(f–i) CCGT and CC constructs do not interact.
(f) YFP–CCGT labeled punctate structures in the cytosol.
(g) Cerulean–CC showed diffuse cytoplasmic distribution in the same cell as (f).
(h) Merged image of (f) and (g).
(i) No restored YFP fluorescence was detected in BiFC combination YN–CCGT + YC–CC.
The insets in (c), (d) and (i) show peroxisome-labeling CFP fluorescence in the same cell as transformation marker at half scale. Scale bar = 20 μm.

involvement of the globular tail in dimerization could occur by two possible pathways. First, a weak dimerization initiated by the coiled-coil region would bring two globular tails into close proximity, which might then provide a second interaction to strengthen the coiled-coil dimerization. Second, the binding of two globular tails to a single organelle surface might orient the two coiled-coil regions side-by-side, thus indirectly enhancing the coiled-coil dimerization. To distinguish between these two possibilities, a chimeric construct, YFP–CCIQGT, was tested for dimerization with the Cerulean–CCGT construct. The six IQ motifs, which form a long and rod-like spacer, can be expected to disrupt the steric symmetry required for inter-tail interaction, which by inference should destabilize dimerization if the first pathway were the case. On the other hand, the presence of this spacer will still allow targeting of CCIQGT construct to occur (Figure 2f), and thus should still stabilize the dimerization if the second pathway were the case. In both FRET and BiFC assays, we detected a stable dimerization between CCIQGT and CCGT constructs (Figures 6 and 7e), which suggested that targeting of the globular tails but not direct interaction between two globular tails stabilizes the coiled-coil dimerization. In fact, the Nfret signal between two globular tails alone was found to be as low as that of the negative control (Figure 6), which suggested that two globular tails do not interact directly.

If targeting were the key to stabilizing the weak MYA1 coiled-coil interaction, we would expect that efficient dimer formation would require simultaneous organelle binding of two globular tails. Consistent with this prediction, different fluorescently labeled CCGT and CC constructs in a FRET assay did not co-localize but exhibited different cytoplasmic distributions (Figure 7f–h). The YFP–CCGT construct labeled punctate structures (Figure 7f), whereas the Cerulean–CC construct showed diffuse distribution in the cytosol (Figure 7g). Similarly, no restored YFP signal in the BiFC combination of YN–CCGT and YC–CC could be detected in 100 cells expressing the CFP transformation indicator (Figure 7i). These results suggested that no stable dimerization occurred between the coiled-coil regions if one of the globular tails was missing.

Discussion

In order to catalyze the rapid long-distance translocation of organelles through plant cells during cytoplasmic streaming, myosin XI proteins have to attach stably to the organelle surface (Li and Nebenführ, 2007) and at the same time walk in

a processive hand-over-hand manner along actin filaments (Tominaga *et al.*, 2003), the latter of which is known to require stable dimerization of two motor proteins (Tominaga *et al.*, 2003). Our study revealed an unexpected inter-dependence of dimerization and organelle binding in myosin XI that suggests an intricate regulation of organelle motility.

Targeting of the globular tail stabilizes myosin XI coiled-coil dimerization

Contrary to the common assumption that myosin XI motors spontaneously form stable dimers through their coiled-coil regions, our BiFC and FRET experiments (Figures 4–7) demonstrated that targeting of the globular tail to the organelle is required for efficient dimerization of the MYA1 coiled-coil region. This requirement is also consistent with data from the Y2H assay as well as the *in vitro* co-purification assay, in which, due to lack of cargo association, coiled-coil regions did not exhibit detectable interactions even in the presence of the globular tail (Figure 3). We postulate that simultaneous binding of two globular tails to the same organelle surface would bring two coiled-coil regions into close proximity, thus indirectly enhancing their dimerization. This postulation is supported by the finding that a coiled-coil region by itself could not dimerize with a coiled-coil region supplemented with the globular tail (Figure 7f–i). Thus, we predicted that the organelle binding of native myosin XI occurs via two globular tails simultaneously, which by inference provides a more stable connection between motor and cargo during their movement through the viscous cytoplasm (Li and Nebenführ, 2008).

The stabilization of myosin XI coiled-coil dimerization by targeting is reminiscent of the dimerization mechanisms recently discovered for other myosins or kinesins, e.g. myosin VI (Altman *et al.*, 2007; Park *et al.*, 2006; Spudich *et al.*, 2007), myosin X (Knight *et al.*, 2005) and kinesin Unc104 (Al-Bassam *et al.*, 2003). However, in those cases, dimerization was strictly dependent on cargo binding. By contrast, myosin XI has a coiled-coil region that is at least partially capable of spontaneous dimerization. This difference may be caused by the relatively large number of hydrophobic residues in core positions of the myosin XI coiled-coil region when compared to myosins VI and X (Knight *et al.*, 2005; Park *et al.*, 2006). Intriguingly, various scenarios have been described for the role of cargo binding in myosin V dimerization, the myosin class that is most similar to myosin XI. On one hand, stable dimerization of human myosin Va appeared to involve the globular tail as neither FLAG-tagged CC nor GT alone, but only a CCGT construct co-precipitated with the full-length myosin Va (Yoshimura *et al.*, 2006). A recent study with the budding yeast myosin V isoform Myo4p also suggested that, although its coiled-coil region was too short to dimerize at physiological concentrations, dimerization could be triggered when the Myo4p globular tail associated with the cargo adaptor She3p (Heuck *et al.*, 2007). On the other hand, dimerization of the budding yeast myosin V isoform Myo2p appeared to be independent of the globular tail as the IQCC construct was able to interact with IQCCGT construct in a Y2H system (Beningo *et al.*, 2000). Thus, the dimerization behaviors of particular myosin classes can vary and should be determined experimentally.

In the case of myosin Va with the alternatively spliced exon B, it has been suggested that a third protein named DYNLL2 stabilizes myosin dimerization by binding to its coiled-coil regions and locking the local structure into a stable dimer (Wagner *et al.*, 2006). In our study, the weak *in vivo* dimerization between MYA1 coiled-coil regions on their own revealed by FRET assays indicated that this scenario is less likely to be the case for myosin XI. Furthermore, the *in vitro* pull-down assay in the presence of Arabidopsis crude protein extracts also failed to detect any other proteins that could facilitate MYA1 tail dimerization.

Imperfect coiled-coil regions in myosin XI lead to weak dimerization

The surprisingly weak dimerization of the long MYA1 coiled-coil region (174 amino acids) on its own is in sharp contrast to the strong dimerization of the short leucine zipper of yeast GCN4 (32 amino acids). We assume that the unstable dimerization between MYA1 coiled-coil regions could be an intrinsic feature of their amino acid sequences. In particular, although a number of core positions (*a* and *d* positions) of the MYA1 coiled-coil region are occupied by small apolar residues that could facilitate dimerization by hydrophobic interactions (Figure 1a and S1b,c), the pronounced lack of attractive electrostatic interactions between the *e* and *g* positions of MYA1 coiled-coil region may lead to the exposure of poorly buried apolar core residues to the aqueous environment, which would dramatically destabilize the hydrophobic interactions between core positions (Figure S1b,c). A similar lack of attractive electrostatic interaction between the *e* and *g* positions has been shown to cause a loosely dimerized zone within the extremely long coiled-coil regions of conventional kinesin (Tripet *et al.*, 1997) and myosin II (Li *et al.*, 2003).

MYA1 coiled-coil dimerization depends predominantly on the first coiled-coil segment (Figures 6 and 7a–d), which appeared to be highly conserved in different Arabidopsis myosin XI isoforms (data not shown). These features imply that weak coiled-coil dimerization might also occur in other myosin XI isoforms. The differential contribution of individual coiled-coil segments to dimerization could be determined by the biochemical differences in their primary sequences (Figure 1a and Appendix S1). Interestingly, other studies with myosin or kinesin coiled-coil regions have also found that their full-length coiled-coil regions were not

necessary to maintain dimerization capability (Park *et al.*, 2006; Vanstraelen *et al.*, 2004). These findings raise the question of whether the entire coiled-coil region of myosin XI is always dimerized. However, according to the visualized stalk length (25 nm) of a tobacco myosin XI dimer (Tominaga *et al.*, 2003), both the CC1 of 11.7 nm and the CC2 of 12.2 nm are likely to stay dimerized.

Dimerization of the coiled-coil region is required for stable myosin XI targeting

In this study, we have demonstrated that dimerization of the coiled-coil region is required for stable targeting of MYA1 (Figure 2). We also observed that the coiled-coil regions of three other myosin XI isoforms in Arabidopsis (i.e. MYA2, XI-I and XI-K) exerted the same effects on the targeting of their globular tails (Figure S2). As these four isoforms represent three of the five clades within the myosin XI subfamily (Avisar *et al.*, 2008), it is likely that dimerization might be a general requirement for stable cargo binding for all myosin XIs. Curiously, another recent study described organelle binding of MYA2 and XI-K globular tails independently of their coiled-coil regions (Reisen and Hanson, 2007). The constructs used in that study were similar to the longer GTplus construct for MYA1 in this study, although we did not detect any difference in organelle binding between MYA1GT and MYA1GTplus constructs. The discrepancy between these two studies is still unresolved, but may point to differences in the affinity of the myosin isoforms for their respective target organelles or differences in the expression systems used. Future identification of the myosin-binding proteins on organelle surfaces should resolve this issue.

However, data from both studies suggest that MYA1 and XI-I at least are not able to bind to organelles stably in monomeric form, but do so when a dimerization interface is provided. This dimerization requirement for stable organelle binding may provide a distinct physiological advantage to the organism. In particular, this mechanism would prevent non-processive monomeric myosins from competing with the fully functional dimers for cognate binding sites on the organelle surface (Figure 8, step 1).

Dimerize, target, go!

Myosin XI is generally assumed to be the molecular motor that drives plant cytoplasmic streaming by pulling a wide variety of organelles through the cytoplasm. The domain structure of myosin XI suggests that actin binding, dimerization and organelle targeting are the central events during assembly of a functional transport complex on actin filaments. However, how these events that occur in three protein domains are coordinated in myosin XI is not clear. In this study, we have found that weak dimerization mediated by the coiled-coil region (Figure 8, step 2) is required for efficient organelle targeting of MYA1 and probably most myosin XI isoforms. In turn, organelle binding of two globular tails (Figure 8, step 3) stabilizes the dimerization of the coiled-coil region by forming a triangle of relatively weak interactions. However, we cannot exclude the alternative possibility for some myosin XI isoforms with higher affinity to organelles that they could attach to organelles as monomers and then dimerize on the organelle surface. Nevertheless, we predict that dimerization and targeting of myosin XI are two synergistic processes. At the same time, it is possible that organelle targeting of the globular tail may activate the actin-based ATPase activity of the motor domain as is known to occur for myosin V (Li *et al.*, 2005b), which subsequently initiates the processive walking of a dimeric myosin XI along the actin track (Figure 8, step 4). Taken together, we propose a model for myosin XI in which its dimerization, organelle targeting and actin-based processive movement occur in a coordinated sequence resulting in efficient regulation of motor activity.

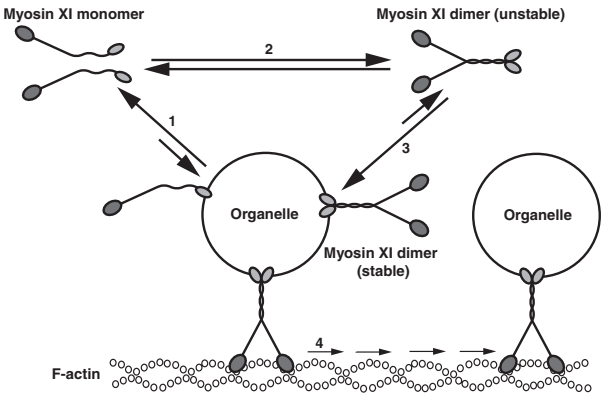

Figure 8. Model for the assembly of the myosin XI–cargo complex on an actin filament.
(1) Myosin XI monomers cannot bind stably to organelles. (2) Two myosin XI monomers form an unstable dimer in the cytosol mediated by coiled-coil interactions. (3) The labile myosin XI dimer stably binds to an organelle with its two globular tail domains. This dual binding to the organelle surface stabilizes the coiled-coil dimerization. (4) Dimeric myosin with the organelle tightly attached to the globular tails moves processively along the actin filament.

Experimental procedures

Yeast two-hybrid assay

Yeast strain Y190 cells were co-transformed with the indicated GAL4 BD bait construct (*TPR1* marker) and the indicated GAL4 AD prey construct (*LEU2* marker), and grown on SD-Trp-Leu plates. Individual colonies of each transformant were patched onto a SD-Trp-Leu-His plate containing 25 mM 3-amino-1,2,4-triazole (3-AT, Sigma-Aldrich, http://www.sigmaaldrich.com/), which blocks leaky expression of the *His3* reporter gene. The plate was then kept at 30°C for 3 days, and β-galactosidase activities for each colony were analyzed by colony-lift filter assay.

In vitro *pull-down assay*

Recombinant protein expression in *E. coli* was performed as described previously (Li *et al.*, 2005a). The *E. coli* BL21 cells (Novagen, http://www.novagen.com) harboring the recombinant expression vectors pET30-His-CCGT or pGEX-GST-CCGT were grown overnight with appropriate antibiotics. The cell cultures were diluted 1:100 into fresh 2YT medium (16 g/L tryptone, 10 g/L yeast extract, 5 g/L NaCl), and were shaken vigorously at 37°C for 3 h. The inducer IPTG was added to a final concentration of 0.1 mM, and the cell cultures were shaken vigorously at 30°C for another 4 h. The cell pellets were disrupted using BugBuster protein extraction buffer (Novagen) containing rLysozyme (Novagen) and Benzonase (Novagen). The initial cell lysates containing His-tagged or GST-tagged CCGT proteins were combined and incubated with Ni-NTA resin (Qiagen, http://www.qiagen.com/) at 4°C for 3 h in the presence or absence of Arabidopsis crude protein extracts, which were obtained as the centrifugation supernatant after thoroughly grinding the Arabidopsis leaf tissue in protein extraction buffer with protease inhibitor cocktail (Roche, http://www.roche-applied-science.com). After the resin was spun down, the supernatant was collected as the resin-unbound fraction. The resin was then intensively washed, and the bound proteins were eluted with 250 mM imidazole and collected as resin-bound fraction. The distribution of His-CCGT and GST-CCGT proteins in resin-unbound or resin-bound fractions was inspected by Western blot analysis using anti-His antibody (Cell Signaling Technology, http://www.cellsignal.com) and anti-GST antibody (a generous gift from Barry Bruce at the University of Tennessee).

Transient expression in Arabidopsis leaves

Dark-green leaves (1 cm long) were detached from 4–8-week-old *Arabidopsis thaliana* Col-0 plants for tungsten particle-mediated DNA bombardment using a PDS-1000 system (Bio-Rad, http://www.bio-rad.com/) according to the procedure described previously (Nelson *et al.*, 2007). When BiFC constructs were bombarded, a construct encoding CFP with a C-terminal type 1 peroxisome targeting signal (Nelson *et al.*, 2007) was co-bombarded as a transformation indicator. After bombardment, the leaves were kept at 28°C in a moist chamber in darkness for 12–16 h prior to microscopic examination.

Fluorescent imaging

Fluorescence microscopy was performed using an Axiovert 200M inverted microscope (Zeiss, http://www.zeiss.com) equipped with filters for YFP and Cerulean fluorescence (Chroma, http://www.chroma.com, filter set 52017). Transformed cells were first identified under a 20× objective before representative cells were observed using a 63× (1.4 NA) plan-apo oil immersion objective. Images were captured using a digital camera (Hamamatsu Orca-ER, http://www.hamamatsu.com) controlled by OPENLAB software (Improvision, http://www.improvision.com). Photographs were subsequently processed for optimal presentation using Adobe® Photoshop® 7.0 (http://www.adobe.com).

FRET measurements by three-channel microscopy

Images were acquired sequentially through Cerulean, FRET and YFP filter channels. The filter sets used for Cerulean were excitation 436/10 nm and emission 465/30 nm, those for FRET were excitation 436/10 nm and emission 535/30 nm, and those for YFP were excitation 500/20 nm and emission 535/30 nm. A dichroic mirror with two transmission windows (476/40 nm and 550/50 nm) was utilized, and Cerulean and YFP emissions were recorded simultaneously after passage through a secondary beam splitter (505 nm). Individual images were background-subtracted prior to FRET analysis. Normalized FRET (Nfret) was calculated using Openlab software (Improvision) on a pixel-by-pixel basis for the entire image using the N_{FRET} algorithm (Xia and Liu, 2001) with experimentally determined bleed-through factors of 0.04 for YFP and 0.5 for Cerulean. The coloration of Nfret images was coded for a range from 0.0 (blue) to 1.0 (red). Areas with substantial image signals in all three channels were selected manually and the mean Nfret values (±SD) for those areas were determined using OPENLAB software (Improvision).

Acknowledgements

We thank colleagues at the University of Tennessee for their kind help; Dr Barry Bruce for the anti-GST antibody, Dr Ana Kitazono for yeast genomic DNA, and Dr Albrecht von Arnim for bacterial expression vectors and use of the gene gun. This work was supported by a National Science Foundation grant (MCB-0416931) to A.N.

Supplementary Material

The following supplementary material is available for this article online:

Figure S1. The coiled-coil region of MYA1 consists of two major coiled-coil sections.

Figure S2. The coiled-coil regions of MYA2, XI-I and XI-K affect the targeting of their globular tails in Arabidopsis leaf epidermis.

Figure S3. BiFC assays indicate that the coiled-coil region mediates MYA1 dimerization in tobacco leaf epidermis.

Figure S4. Dimerization of MYA1 coiled-coil constructs in tobacco leaf epidermis measured by FRET.

Appendix S1. Experimental procedures (bioinformatics analysis, plasmid construction, transient expression in tobacco leaves), results and discussion (additional considerations of MYA1 coiled-coil prediction, prediction of coiled-coil dimerization strength based on primary sequence).

This material is available as part of the online article from http://www.blackwell-synergy.com

Please note: Blackwell Publishing are not responsible for the content or functionality of any supplementary materials supplied by the authors. Any queries (other than missing material) should be directed to the corresponding author for the article.

References

Al-Bassam, J., Cui, Y., Klopfenstein, D., Carragher, B.O., Vale, R.D. and Milligan, R.A. (2003) Distinct conformations of the kinesin Unc104 neck regulate a monomer to dimer motor transition. *J. Cell Biol.* **163**, 743–753.

Altman, D., Goswami, D., Hasson, T., Spudich, J.A. and Mayor, S. (2007) Precise positioning of myosin VI on endocytic vesicles in vivo. *PLoS Biol.* **5**, e210.

Avisar, D., Prokhnevsky, A.I., Makarova, K.S., Koonin, E.V. and Dolja, V.V. (2008) Myosin XI-K is required for rapid trafficking of Golgi stacks, peroxisomes and mitochondria in leaf cells of *Nicotiana benthamiana*. *Plant Physiol.* **146**, 1098–1108.

Beningo, K.A., Lillie, S.H. and Brown, S.S. (2000) The yeast kinesin-related protein Smy1p exerts its effects on the class V myosin Myo2p via a physical interaction. *Mol. Biol. Cell*, **11**, 691–702.

Cole, R.A. and Fowler, J.E. (2006) Polarized growth: maintaining focus on the tip. *Curr. Opin. Plant Biol.* **9**, 579–588.

Dixit, R., Cyr, R. and Gilroy, S. (2006) Using intrinsically fluorescent proteins for plant cell imaging. *Plant J.* **45**, 599–615.

Foth, B.J., Goedecke, M.C. and Soldati, D. (2006) New insights into myosin evolution and classification. *Proc. Natl Acad. Sci. USA*, **103**, 3681–3686.

Goodin, M.M., Chakrabarty, R., Banerjee, R., Yelton, S. and DeBolt, S. (2007) New gateways to discovery. *Plant Physiol.* **145**, 1100–1109.

Hashimoto, K., Igarashi, H., Mano, S., Nishimura, M., Shimmen, T. and Yokota, E. (2005) Peroxisomal localization of a myosin XI isoform in *Arabidopsis thaliana*. *Plant Cell Physiol.* **46**, 782–789.

Heuck, A., Du, T.G., Jellbauer, S., Richter, K., Kruse, C., Jaklin, S., Müller, M., Buchner, J., Jansen, R.P. and Niessing, D. (2007) Monomeric myosin V uses two binding regions for the assembly of stable translocation complexes. *Proc. Natl Acad. Sci. USA*, **105**, 19778–19783.

Houtman, D., Pagonabarraga, I., Lowe, C.P., Esseling-Ozdoba, A., Emons, A.M.C. and Eiser, E. (2007) Hydrodynamic flow caused by active transport along cytoskeletal elements. *Europhys. Lett.* **78**, 18001.

Hu, C.D., Chinenov, Y. and Kerppola, T.K. (2002) Visualization of interactions among bZIP and Rel family proteins in living cells using bimolecular fluorescence complementation. *Mol. Cell*, **9**, 789–798.

Jedd, G. and Chua, N.H. (2002) Visualization of peroxisomes in living plant cells reveals acto-myosin-dependent cytoplasmic streaming and peroxisome budding. *Plant Cell Physiol.* **43**, 384–392.

Jiang, S. and Ramachandran, S. (2004) Identification and molecular characterization of myosin gene family in *Oryza sativa* genome. *Plant Cell Physiol.* **45**, 590–599.

Kammerer, R.A., Schulthess, T., Landwehr, R., Lustig, A., Engel, J., Aebi, U. and Steinmetz, M.O. (1998) An autonomous folding unit mediates the assembly of two-stranded coiled coils. *Proc. Natl Acad. Sci. USA*, **239**, 591–597.

Kinkema, M. and Schiefelbein, J.A. (1994) A myosin from a higher plant has structural similarities to class V myosins. *J. Mol. Biol.* **239**, 591–597.

Knight, P.J., Thirumurugan, K., Yu, Y., Wang, F., Kalverda, A.P., Stafford, W.F. III, Sellers, J.R. and Peckham, M. (2005) The predicted coiled-coil domain of myosin 10 forms a novel elongated domain that lengthens the head. *J. Biol. Chem.* **280**, 34702–34708.

Krendel, M. and Mooseker, M.S. (2005) Myosins: tails and heads of functional diversity. *Physiology*, **20**, 239–251.

Li, J.F. and Nebenführ, A. (2007) Organelle targeting of myosin XI is mediated by two globular tail subdomains with separate cargo binding sites. *J. Biol. Chem.* **282**, 20593–20602.

Li, J.F. and Nebenführ, A. (2008) The tail that wags the dog: the globular tail domain defines the function of myosin V/XI. *Traffic*, **9**, 290–298.

Li, Y., Brown, J.H., Reshetnikova, L., Blazsek, A., Farkas, L., Nyitray, L. and Cohen, C. (2003) Visualization of an unstable coiled coil from the scallop myosin rod. *Nature*, **424**, 341–345.

Li, J.F., Qu, L.H. and Li, N. (2005a) Tyr152 plays a central role in the catalysis of 1-aminocyclopropane-1-carboxylate synthase. *J. Exp. Bot.* **56**, 2203–2210.

Li, X.D., Ikebe, R. and Ikebe, M. (2005b) Activation of myosin Va function by melanophilin, a specific docking partner of myosin Va. *J. Biol. Chem.* **280**, 17815–17822.

Lupas, A., Van Dyke, M. and Stock, J. (1991) Predicting coiled coils from protein sequences. *Science*, **252**, 1162–1164.

Mason, J.M. and Arndt, K.M. (2004) Coiled coil domains: stability, specificity, and biological implications. *Chembiochem*, **5**, 170–176.

McDonnell, A.V., Jiang, T., Keating, A.E. and Berger, B. (2006) Paircoil2: improved prediction of coiled coils from sequence. *Bioinformatics*, **22**, 356–358.

Nebenführ, A., Gallagher, L.A., Dunahay, T.G., Frohlick, J.A., Mazurkiewicz, A.M., Meehl, J.B. and Staehelin, L.A. (1999) Stop-and-go movements of plant Golgi stacks are mediated by the acto-myosin system. *Plant Physiol.* **121**, 1127–1141.

Nelson, B.K., Cai, X. and Nebenführ, A. (2007) A multicolored set of in vivo organelle markers for co-localization studies in Arabidopsis and other plants. *Plant J.* **51**, 1126–1136.

Ojangu, E.L., Jarve, K., Paves, H. and Truve, E. (2007) *Arabidopsis thaliana* myosin XIK is involved in root hair as well as trichome morphogenesis on stems and leaves. *Protoplasma*, **230**, 193–202.

Park, H., Ramamurthy, B., Travaglia, M., Safer, D., Chen, L.Q., Franzini-Armstrong, C., Selvin, P.R. and Sweeney, H.L. (2006) Full-length myosin VI dimerizes and moves processively along actin filaments upon monomer clustering. *Mol. Cell*, **21**, 331–336.

Peremyslov, V.V., Prokhnevsky, A.I., Avisar, D. and Dolja, V.V. (2008) Two class XI myosins function in organelle trafficking and root hair development in *Arabidopsis*. *Plant Physiol.* **146**, 1109–1116.

Reddy, A.S. and Day, I.S. (2001) Analysis of the myosins encoded in the recently completed *Arabidopsis thaliana* genome sequence. *Genome Biol.* **2**, 0024.

Reichelt, S., Knight, A.E., Hodge, T.P., Baluska, F., Samaj, J., Volkmann, D. and Kendrick-Jones, J. (1999) Characterization of the unconventional myosin VIII in plant cells and its localization at the post-cytokinetic cell wall. *Plant J.* **19**, 555–567.

Reisen, D. and Hanson, H.R. (2007) Association of six YFP–myosin XI-tail fusions with mobile plant cell organelles. *BMC Plant Biol.* **7**, 6.

Rizzo, M.A., Springer, G.H., Granada, B. and Piston, D.W. (2004) An improved cyan fluorescent protein variant useful for FRET. *Nat. Biotechnol.* **22**, 445–449.

Romagnoli, S., Cai, G., Faleri, C., Yokota, E., Shimmen, T. and Cresti, M. (2007) Microtubule- and actin filament-dependent motors are distributed on pollen tube mitochondria and contribute differently to their movement. *Plant Cell Physiol.* **48**, 345–361.

Rose, A., Manikantan, S., Schraegle, S.J., Maloy, M.A., Stahlberg, E.A. and Meier, I. (2004) Genome-wide identification of Arabidopsis coiled-coil proteins and establishment of the ARABI-COIL database. *Plant Physiol.* **134**, 927–939.

Shimmen, T. (2007) The sliding theory of cytoplasmic streaming: fifty years of progress. *J. Plant. Res.* **120**, 31–43.

Shimmen, T. and Yokota, E. (1994) Physiological and biochemical aspects of cytoplasmic streaming. *Int. Rev. Cytol.* **155**, 97–139.

Spudich, G., Chibalina, M.V., Au, J.S., Arden, S.D., Buss, F. and Kendrick-Jones, J. (2007) Myosin VI targeting to clathrin-coated structures and dimerization is mediated by binding to disabled-2 and PtdIns(4,5)P_2. *Nat. Cell Biol.* **9**, 176–183.

Tominaga, M., Kojima, H., Yokota, E., Orii, H., Nakamori, R., Katayama, E., Anson, M., Shimmen, T. and Oiwa, K. (2003) Higher plant myosin XI moves processively on actin with 35 nm steps at high velocity. *EMBO J.* **22**, 1263–1272.

Tripet, B., Vale, R.D. and Hodges, R.S. (1997) Demonstration of coiled-coil interactions within the kinesin neck region using synthetic peptides. Implications for motor activity. *J. Biol. Chem.* **272**, 8946–8956.

Van Gestel, K., Köhler, R.H. and Verbelen, J.P. (2002) Plant mitochondria move on F-actin, but their positioning in the cortical

cytoplasm depends on both F-actin and microtubules. *J. Exp. Bot.* **53**, 659–667.

Vanstraelen, M., Torres Acosta, J.A., De Veylder, L., Inze, D. and Geelen, D. (2004) A plant-specific subclass of C-terminal kinesins contains a conserved A-type cyclin-dependent kinase site implicated in folding and dimerization. *Plant Physiol.* **135**, 1417–1429.

Wagner, W., Fodor, E., Ginsburg, A. and Hammer, J.A. III (2006) The binding of DYNLL2 to myosin Va requires alternatively spliced exon B and stabilizes a portion of the myosin's coiled-coil domain. *Biochemistry*, **45**, 11564–11577.

Wang, Z. and Pesacreta, T.C. (2004) A subclass of myosin XI is associated with mitochondria, plastids, and the molecular chaperone subunit TCP-1α in maize. *Cell Motil. Cytoskeleton*, **57**, 218–232.

Xia, Z. and Liu, Y. (2001) Reliable and global measurement of fluorescence resonance energy transfer using fluorescence microscopes. *Biophys. J.* **81**, 2395–2402.

Yoshimura, A., Fujii, R., Watanabe, Y., Okabe, S., Fukui, K. and Takumi, T. (2006) Myosin-Va facilitates the accumulation of mRNA/protein complex in dendritic spines. *Curr. Biol.* **16**, 2345–2351.

